CORROSION SCIENCE AND TECHNOLOGY, Vol.2, No.2(2003), pp.59~67

Effect of Precipitate on the Electrochemical Potentiokinetic Reactivation Behaviors of Stainless Steels and Nickel Base Alloys

Tsung-Feng Wu, Tzu-Sheng Chen, and Wen-Ta Tsai

Department of Materials Science and Engineering
National Cheng Kung University

Electrochemical potentiokinetic reactivation (EPR) tests are used to evaluate the degree of sensitization (DOS) of stainless steels and nickel base alloys. The validity of EPR test to detect DOS of these alloys, however, depends on the electrolyte composition employed. The existence of precipitates such as NbC, and TiC, etc. in the alloys also affects the reactivation behaviors of these alloys. In this investigation, the reactions involved during EPR processes are analyzed. In 0.5 M H_2SO_4 + 0.01 M KSCN electrolyte, a reactivation peak associated with the localized attack around NbC, different from that of intergranular corrosion, is observed for the solution annealed 347 SS. For solution annealed Alloy 600, matrix corrosion and localized attack around TiC with distinct anodic peaks appeared in the EPR curves are seen in the H_2SO_4 + KSCN electrolyte. With proper adjustment of electrolyte composition, the contribution from intergranular corrosion, as a result of chromium carbide precipitation along the grain boundaries, can be distinguished from the matrix and localized corrosion for the sensitized Alloy 600.

Keywords : *Electrochemical potentiokinetic reativation (EPR), intergranualr corrosion, precipitates, 347 SS, nickel base alloys.*

1. Introduction

EPR technique for passivated stainless steel was proposed in the 1960s as a method to detect stainless steel' s the susceptibility to intergranular attack (IGA) of stainless steels.[1-3] The susceptibility was produced by chromium depletion in the vicinity of the grain boundaries, which resulted from chromium carbides precipitation of numerous stainless steels following welding operations and other thermal exposures between 500 to 800°C produced this susceptibility.[4),5] Therefore, these depleted regions might be subject to rapid preferential attack. To date, the EPR technique, proposed by Prazak[1] and Clarke et al.,[6),7] then developed by Novak[3] and others,[2),8),9] has become the standard method to detect the degrees of sensitization in 304 and 304L SSs.[10),11] The validity of EPR, however, is seldom reported for the evaluation of degree of sensitization in Nb-containing 347 SS.

The EPR test technique has also been applied to evaluate the susceptibility of high-nickel alloys to intergranular corrosion.[12)-14] However, other corrosion types, except beside intergranular corrosion, other types of corrosion were observed after single-loop SL-EPR (SL-EPR) test. In other words, the SL-EPR reactivation curves for nickel base alloys obtained from SL-EPR were involved intomight involve several kinds of reactions. For Alloy 600, for example, pitting corrosion associated with TiC might take part in the reactivation behavior.[15] The rather complicated reactivation behavior of nickel base alloy as a function of electrolyte composition is thus of interest and investigated. The validity of SL-EPR for detecting the degree of sensitization of Nb-stabilized 347 SS and Alloy 600 is also attempted.

2. Experimental

The chemical compositions of 304 SS, 347 SS and Alloy 600 along with 304 SS (for comparison) are listed in Table 1. . Two different thermal treatments were applied to these alloys, namely, solution annealing and thermal aging to facilitate chromium carbide formation (Table 2). Following heat treatment, the specimens were ground, polished and rinsed in distilled water prior to metallographical, chemical and electrochemical tests.

Chemical tests were conducted to examine the susceptibility to intergranular corrosion of 304 SS, 347 SS and Alloy 600. For 304 and 347 SSs, oxalic acid etch test(ASTM A262 A)[16] was employed, while modified

Table 1. Chemical compositions of type 304SS, 347 SS and Alloy 600 used (wt%).

	Fe	Cr	Ni	C	Si	Mn	Cu	P	S	N	Nb
304 SS		18.3	9.22	0.03	0.51	1.88	2.08	0.029	0.008	0.012	-
347 SS	68.8	18.2	10.6	0.028	0.42	1.17	-	0.012	0.0004	0.14	0.64
Alloy 600	8.48	16.19	74.55	0.023	0.25	0.31	0.19	-	-	-	-

Table 2. Heat treatments applied for 304SS, 347 SS and Alloy 600.

Materials	Specimen designation	Heat treatment
Alloy 600	600-SA	1150℃/1h + water quench (SA)
	600-15	SA + 704℃/15h + water quench
304 SS, 347 SS	304-SA, 347-SA	1100℃/0.5h + water quench (SA)
	304-15, 347-15	SA + 650℃/15h + water quench

Table 3. Parameters used for SL-EPR test for 304SS, 347 SS and Alloy 600.

Parameters		Alloy 600	304 SS, 347 SS
Electrolyte	H_2SO_4 concentration (M)	0.5	0.5
	KSCN concentration (M)	0.005~0.5	0.01
Passivation	Potential (mV/SCE)	+400	+200
	Time (s)	120	120
Reactivation	Potential range (mV/SCE)	+400→-375	+200→-450
	Scan rate (mV/s)	1.67	1.67

Huey test[17-19] (in boiling 25 % HNO_3 solution) was used for Alloy 600. Following the tests, the surface morphology of the specimens were then examined via scanning electron microscopy (SEM) and optical microscopy (OM).

Reactivation polarization behaviors of 304 SS, 347 SS and Alloy 600 in the H_2SO_4 + KSCN electrolytes were conducted via the SL-EPR test. The electrolyte compositions and parameters of SL-EPR tests are demonstrated in Table 3. Subsequent to each EPR test, the specimen was examined using OM.

3. Results and discussion

3.1 Etched microstructure

3.1.1 304 SS and 347 SS

The optical micrographs for the solution annealed (SA, 1100℃/0.5h) and thermal treated (SA + 650℃/15h) 304 SS and 347 SS, after oxalic acid etch test, are shown in Figs. 1 and 2, repectively. For 304 SS, as expected and

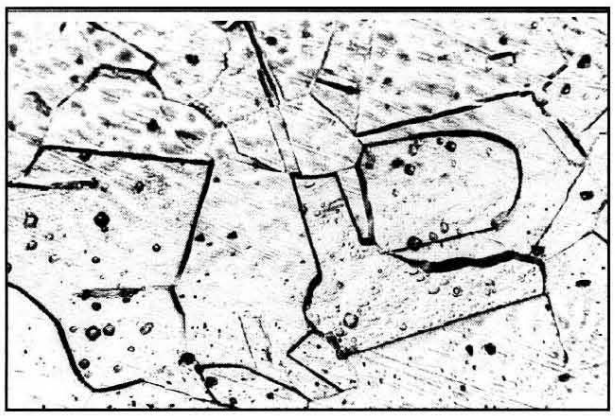

(a)

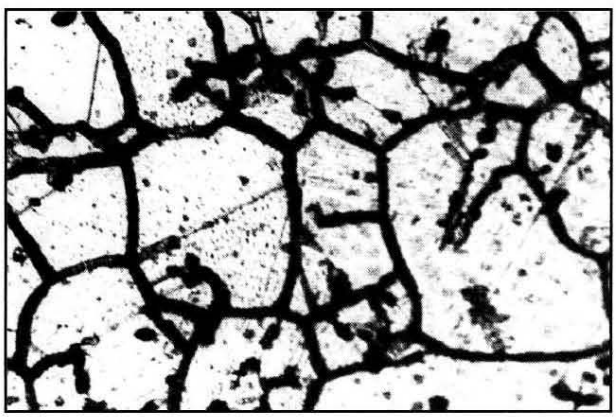

(b) 25 μm

Fig. 1. Micrographs of 304 SS with different thermal treatments after oxalic acid etch test, (a) 304-SA (1100℃/0.5h) (b)304-15 (SA+650℃/15h)

demonstrated in Fig. 1, the step structure was revealed in solution annealed 304 SS while ditch structure in 304 SS with 650℃/15h thermal treatment. In fact, thermal treatment at 650℃ for 15h resulted in a sensitized microstructure in 304 SS. However, only step structure was observed in both 347 SS specimens, either solution annealed or thermal treated at 650℃/15h (Fig. 2). Clearly, the alloying of Nb sufficiently prevented sensitization of austenitic stainless steel.

(a)

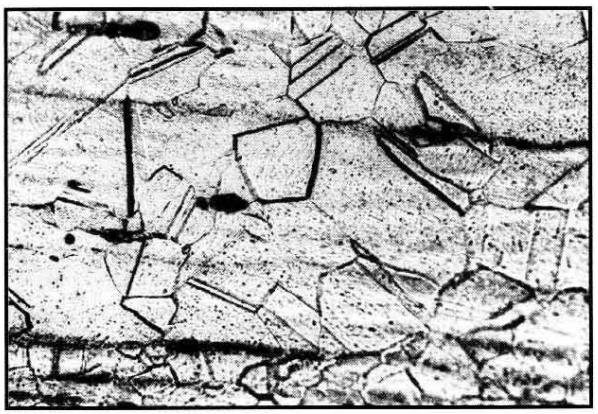

(b) 25 μm

Fig. 2. Micrographs of 347 SS with different thermal treatments after oxalic acid etch test, (a) 347-SA (1100℃/0.5h) (b)347-15 (SA+650℃/15h)

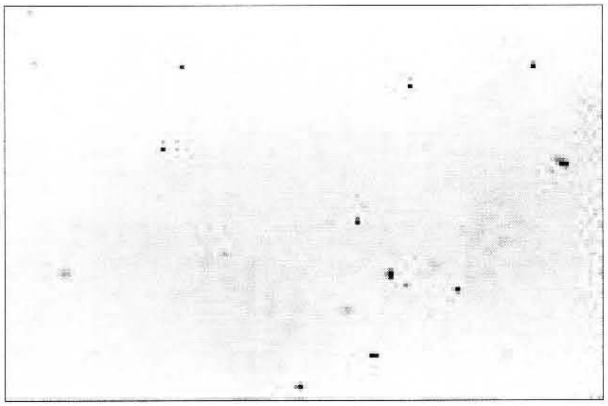

(a)

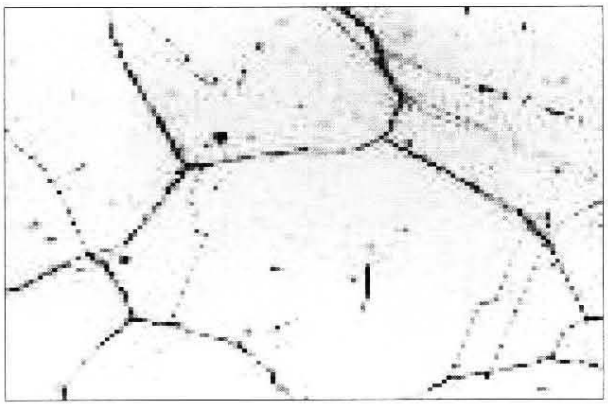

(b) 100 μm

Fig. 3. Metallogrphs showing carbide precipi- tation of Alloy 600 with different thermal treatments, electrolytically etched in $H_3PO_4 : H_2O = 8 : 1$ electrolyte, (a) 600-SA (1150℃/1h) (b)600-15 (SA+704℃/15h)

3.1.2 Alloy 600

The precipitation of carbide and its distribution in Alloy 600 were examined by electrolytical etched etching in $H_3PO_4 : H_2O = 8 : 1$ electrolyte. Fig. 3 shows that carbide precipitation was negligible for Alloy 600 with solution annealing treatment. Extensive grain boundary carbide precipitation, however, was observed for the specimen heat treated at 704℃/15h Regardless of the heat treatment, fine, rectangular precipitates were observed in both specimens. These precipitates were identified as TiC from energy dispersive soectroscopy as well as from their shape and tincture of orange color.

The degree of sensitization of Alloy 600 was examined by chemical test. The morphologies of Alloy 600 with different thermal treatment after modified Huey's test were shown in Fig. 4. Intergranular corrosion was not found in the solution annealed (1100℃/1h) Alloy 600, indicating not being sensitized For the specimen aged at 704℃ for 15h after solution annealing, however, grain dropping out of the surface resulting from grain boundary corrosion was seen. By comparing with those in Fig. 3, the result indicated that intergranular corrosion was related to grain boundary carbide precipitation. Apparently, Alloy 600 subjected to 704℃/15h thermal treatment was sensitized.

3.2 SL-EPR tests

3.2.1 304 SS

Fig. 5(a) shows the SL-EPR polarization curves of 304 SS with different heat treatments, which were conducted in 0.5M H_2SO_4 + 0.01M KSCN solution, It was obvious that a humped reactivation curve appeared in the sensitized 304SS while not in solution annealed 304 SS. The surface appearances of these two specimens after SL-EPR test were depicted in Figs. 5(b) and (c). Almost no corrosion,

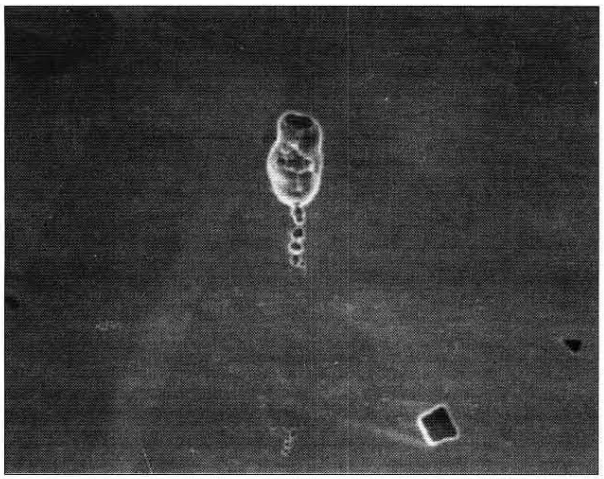

(a)

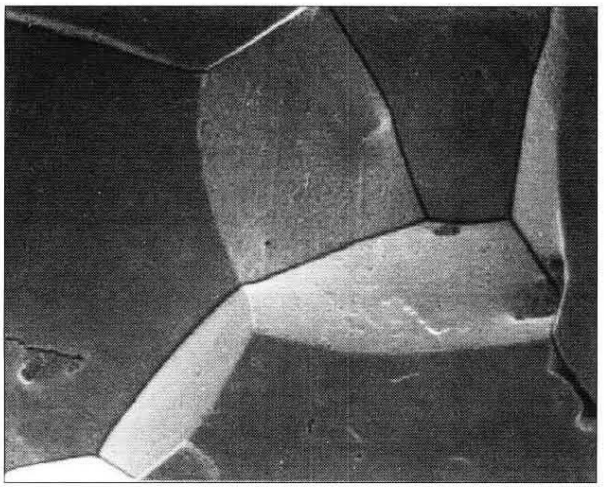

(b)

Fig. 4. SEM micrographs showing the surface appearances of Alloy 600 with different thermal treatments after modified Huey test, (a) 600-SA (1150℃/1h) (b)600-15 (SA+704℃/15h)

except some pits, was seen on the solution annealed 304 SS after EPR test, However, apparent grain boundary corrosion was found on the sensitized 304 SS. The results were no different from those reported in the literature.[6),20)]

3.2.2 Alloy 600

Fig. 6(a) illustratesd the SL-EPR polarization curves of Alloy 600 with different heat treatments, which were conducted in 0.5M H_2O_4 + 0.005M KSCN solution, Notably, regardless of the heat treatment, a hump with two peaks appeared in each reactivation polarization curve. This differs significantly from that occurreds in the "clea n" 304 SS where no reactivation hump was discovered

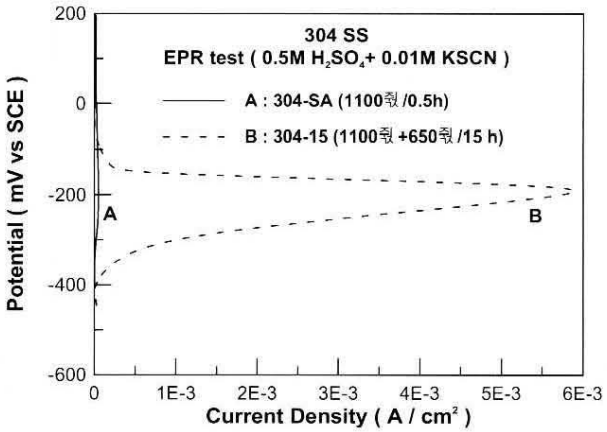

(a)

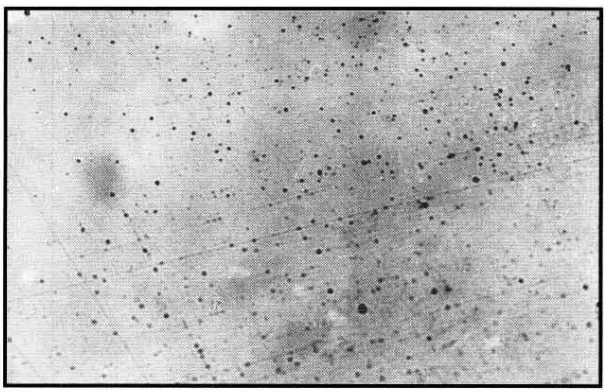

(b)

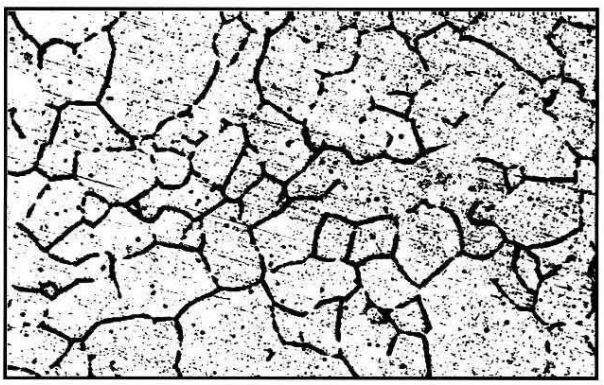

(c)

Fig. 5. Morphologies and polarization curves of 304 SS with different thermal treatment after SL-EPR test in 0.5M H_2SO_4 + 0.01M KSCN solution, (a) polarization curves, morphologies of (b)304-SA and (c) 304-15.

for the non-sensitized alloy (Fig 5(a)). Despite the similarity in the reactivation curves for both specimens, the

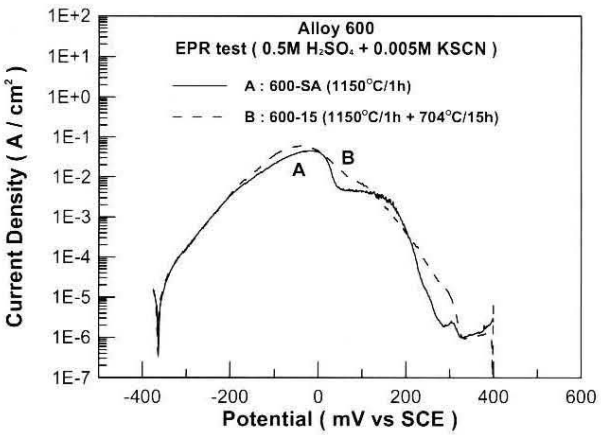

(a)

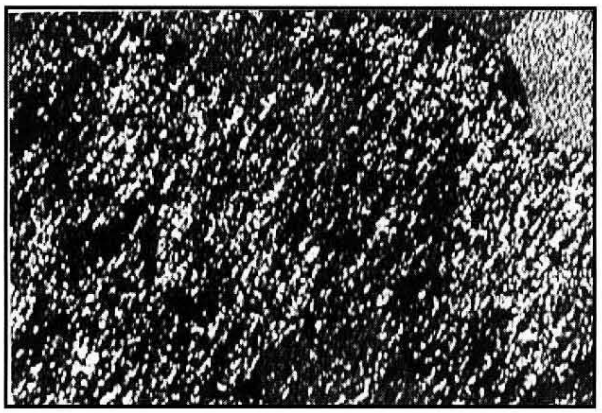

(b)

100 μm

(c)

Fig. 6. Morphologies and polarization curves of Alloy 600 with different thermal treatment after SL-EPR test in 0.5M H2SO4 + 0.005M KSCN solution, (a) polarization curves, morphologies of (b)600-SA and (c) 600-15.

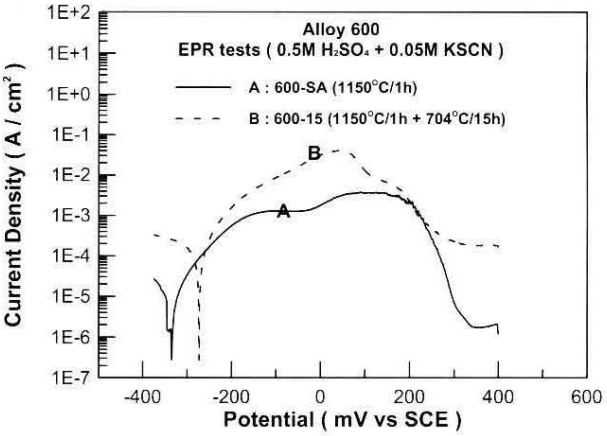

(a)

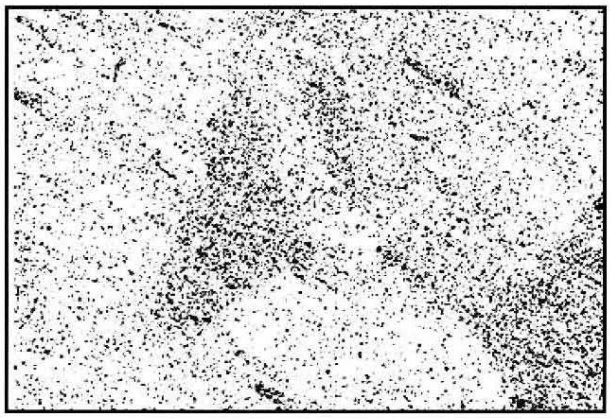

(b)

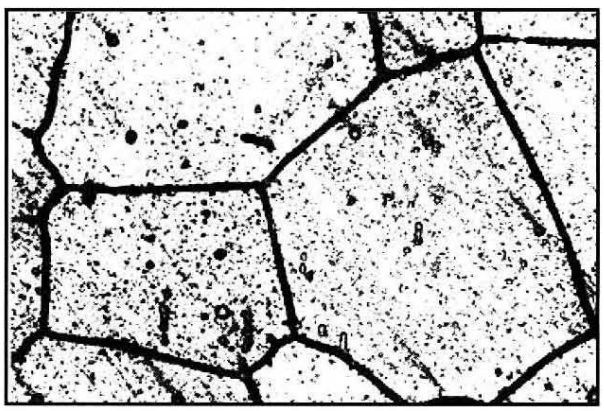

100 μm

(c)

Fig. 7. Morphologies and polarization curves of Alloy 600 with different thermal treatment after SL-EPR test in 0.5M H_2SO_4 + 0.05M KSCN solution, (a) polarization curves, morphologies of (b)600-SA and (c) 600-15.

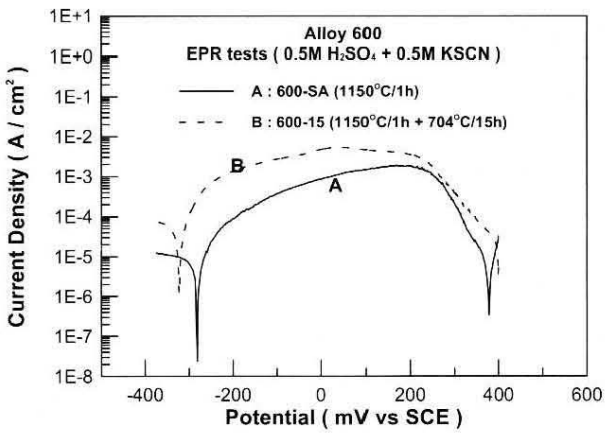

(a)

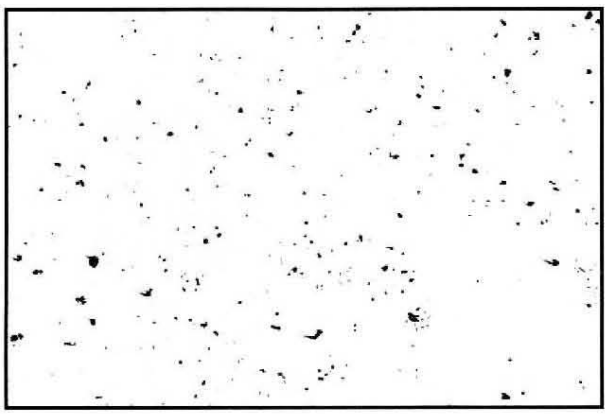

(b)

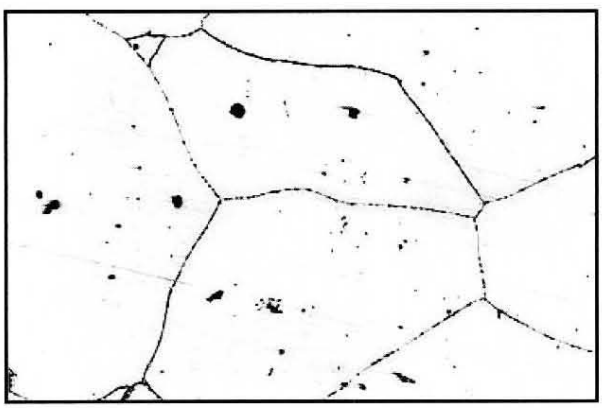

(c)

Fig. 8. Morphologies and polarization curves of Alloy 600 with different thermal treatment after SL-EPR test in 0.5M H_2SO_4 + 0.5M KSCN solution, (a) polarization curves, morphologies of (b)600-SA and (c) 600-15.

morphologies were not exactly the same. As can seen as in Fig. 6(b) severe matrix corrosion was observed in the non-sensitized Alloy 600. For sensitized Alloy 600, intergranualar corrosion, which still could be distinguished from matrix corrosion, was depicted in Fig. 6(c).

The effect of KSCN concentration on the reactivation behaviors was explored. The SL-EPR polarization curves and morphologies after tests in 0.5M H_2SO_4 + 0.05M KSCN solution were demonstrated in Fig. 7. The reactivation polarization curves could be distinguished between sensitized and non-sensitized specimens which were different with those in Fig. 6(a) (in 0.5M H_2SO_4 + 0.005M KSCN). Two apparent reactivation peaks (about +150 and − 150 mV/SCE, respectively) were seen in such electrolyte for non-sensitized Alloy 600, while three peaks for sensitized Alloy 600. It seemed to imply that there might be two separated reactions in reactivation process for non-sensitized Alloy 600, while three for sensitized specimen. The additional peak for sensitized Alloy 600, revealed in at +30 mV/SCE, was considered being contributed by intergranular corrosion. The morphologies depicted in Figs. 7(b) and (c), after SL-EPR tests in 0.5M H_2SO_4 + 0.05M KSCN solution, showed less degree of matrix corrosion compared with those conducted in 0.5M H_2SO_4 + 0.005M KSCN solution, as can seen in Figs. 6(b) and (c).

Fig. 8(a) shows the SL-EPR polarization curves in 0.5M H_2SO_4 + 0.5M KSCN solution. At such a high concentration of KSCN, though there still exhibited wide anodic humps for both heat treated Alloy 600, the respective peaks as revealed in Figs. 6(a) and 7 (a) became less distinguishable. Nevertheless, the sensitized Alloy 600 had a higher anodic current density, compared with the solution annealed specimen, and the maximum appeared around +30 mV. The associated micrographs after EPR tests are shown in Figs. 8(b) and (c) for the non-sensitized and the sensitized Alloy 600, respectively. Grain boundary corrosion was seen for the sensitized alloy. As can be seen as in Figs. 8(b) and (c), matrix corrosion was reduced as the concentration of KSCN was increased to 0.5 M.

Coupled with reactivation termination test,[15] the reactivation polarization curves were dissociated into two or three partial reactions depending on whether Alloy 600 was sensitized or not. Fig. 9(a) illustrates a schematic diagram, which indicates that the reactivation polarization curve consisted of pitting corrosion at relative higher anodic potential and matrix corrosion at lower anodic potential within the solution annealed or non-sensitized Alloy 600, The occurrence of pitting corrosion was generally associated with the precipitates such as TiC, etc., present in the matrix. For sensitized Alloy 600, an inter-

mediate peak associated with intergranular corrosion and having the highest anodic current density existed in the deconvolution diagram (Fig. 9(b)). With proper adjustment of electrolyte composition, the contribution to the total reactivation current density from intergranular corrosion, as a result of chromium carbide precipitation along the grain boundaries, can could be distinguished from the matrix and localized corrosion for the sensitized Alloy 600.

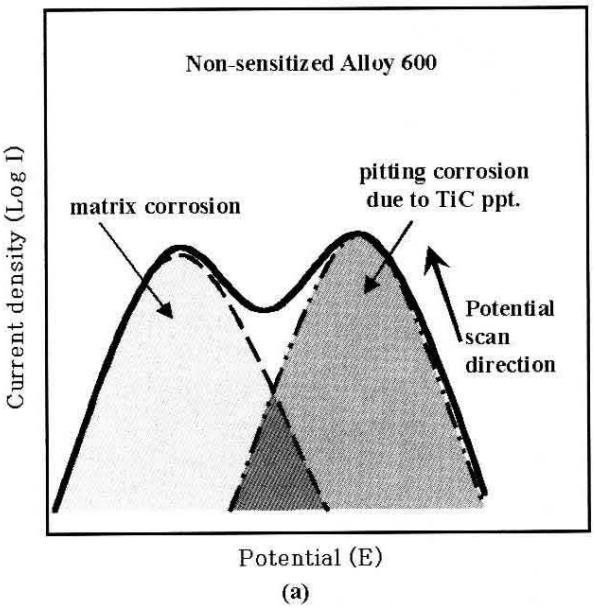

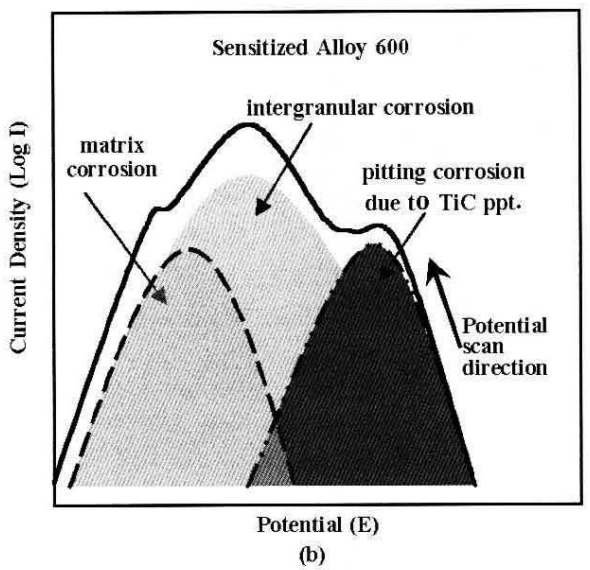

Fig. 9. Schematic deconvolution diagram of the reactivation polarization curves of Alloy 600 with different thermal treatment in H_2SO_4 + KSCN solutions, (a) non-sensitized Alloy 600 (b) sensitized Alloy 600.

3.2.3 347 SS

The SL-EPR polarization curves of 347 SS with different heat treatments, conducted in 0.5M H_2SO_4 +

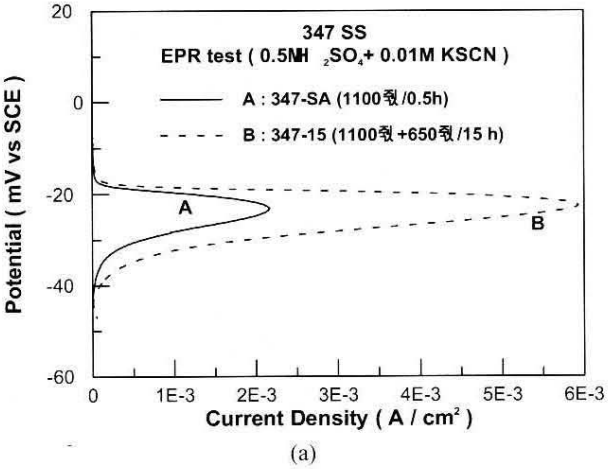

(a)

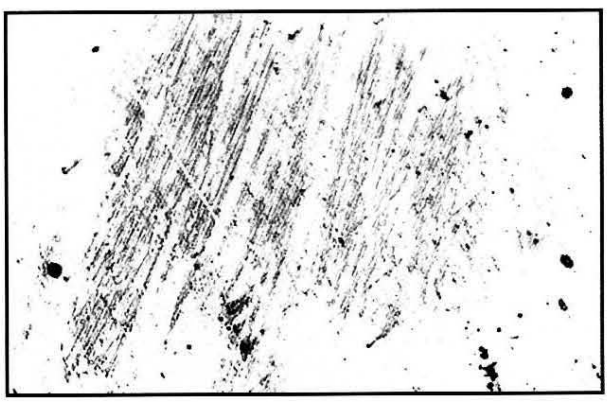

(b)

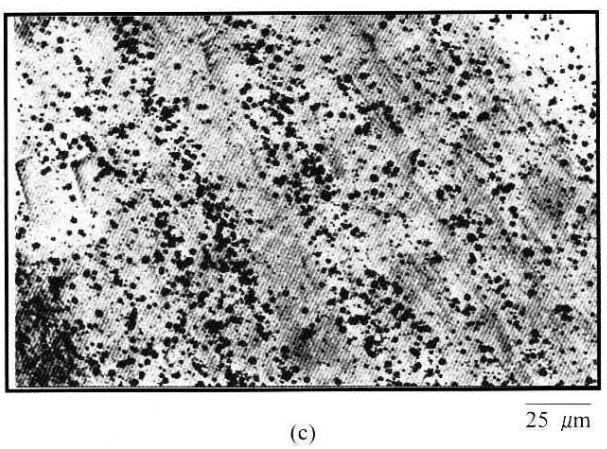

(c)

Fig. 10. Morphologies and polarization curves of 347 SS with different thermal treatment after SL-EPR test in 0.5M H_2SO_4 + 0.01M KSCN solution, (a) polarization curves, morphologies of (b)347-SA and (c) 347-15.

0.01M KSCN solution, are shown in Fig. 10(a). An apparent reactivation hump appeared in each SL-EPR curves. It was interesting to note that an anodic peak with significant magnitude was observed for the solution annealed 347 SS, which was quite unusual as compared with that of the solution annealed 304 SS (Fig. 5(a)). Furthermore, as mentioned early, thermal treatment at 650℃ for 15h did not cause a sensitized microstructure for the Nb-stabilized 347 SS. However, a peak still existed in the reactivation curve. The reactivation peaks appeared in Fig. 10(a) should not be attributed to grain boundary corrosion. The micrographs showing the surface morphologies, after SL-EPR tests, of 347 SS subjected to solution annealing and 650℃/15h heat treatment, respectively, did nor reveal any evidence of grain boundary corrosion. Only pits were seen on the specimen surfaces, as revealed in Figs. 10(b) and (c). The reactivation peaks, appeared in Fig. 10(a), were thus believed to associate with pitting corrosion. Similar observation on the contribution of pitting corrosion to the SL-EPR curve had been reported by Majidi and Streicher.[20] Detail microscopic examination further indicated that pitting corrosion occurred around NbC precipitates. The results indicated that SL-EPR might not be adequate to detect the degree of sensitization of 347 SS.

By superimposing Figs. 5(a) and 10(a), it was found that the reactivation peak for grain boundary corrosion was different from that of pitting corrosion, (see Fig. 11). The potential associated with pitting corrosion was higher than that of grain boundary corrosion. The potential sequence with respect to the occurrence of pitting corrosion and grain boundary corrosion was similar to that found in Alloy 600 in SL-EPR test. The contribution to the anodic reactivation current density from grain boundary corrosionor pitting corrosion as a function of potential is demonstrated in the schematic diagram in Fig. 12. Unlike that of Alloy 600, the contribution from matrix corrosion for austenitic stainless steel was insignificant. No peaks associated with matrix corrosion were observed in the SL-EPR curves of the austenitic stainless steels determined in this investigation.

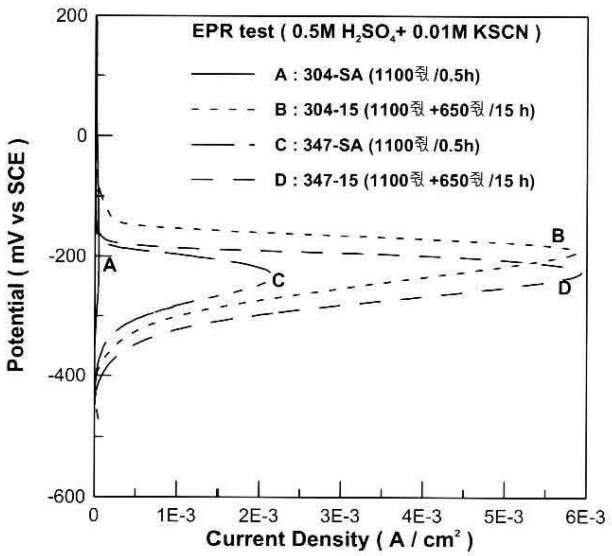

Fig. 11. SL-EPR polarization curves of 304 SS and 347 SS with different thermal treatments in 0.5M H_2SO_4 + 0.01M KSCN solution.

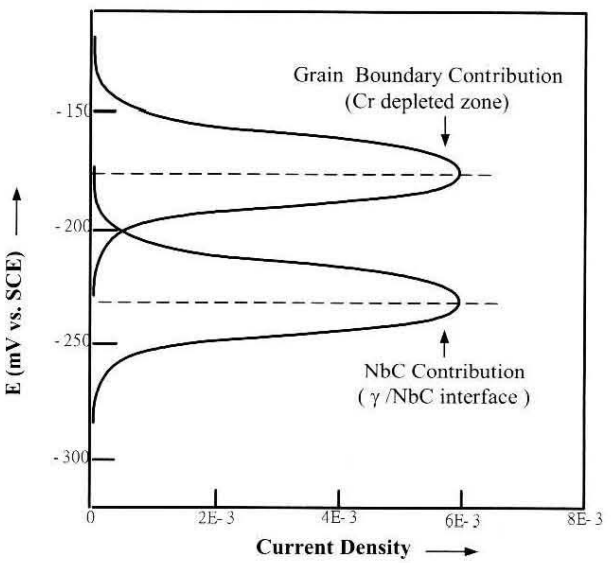

Fig. 12. Schematic diagram showing the shift of the reactivation peak potential for sensitized 304 SS and 347 SS in H_2SO_4 +KSCN solutions.

4. Conclusions

1. For sensitized Alloy 600, three anodic peaks appeared in the SL-EPR reactivation polarization curve tested in the H_2SO_4 + KSCN electrolyte. The peak associated with grain boundary corrosion was located at a potential in between the two peaks for pitting corrosion and matrix corrosion. For non-sensitized Alloy 600, the reactivation hump still existed, consisting of one peak for pitting corrosion at a higher potential and the other for matrix corrosion at a lower potential.

2. For the Nb-stabilized and non-sensitized 347 SS, the reactivation peak appeared in the SL-EPR curve was associated with pitting corrosion around NbC.

References

1. M. Prazak, *Corrosion*, **19**, 75t (1963).
2. F. Duffaut, J. P. Pouzet, and P. Lacombe, *Corros. Sci.*, **6**, 83 (1966).
3. P. Novak, R. Stefec, and F. Franz, *Corrosion*, **31**, 344 (1975).
4. R. L. Cowan and C. S. Tedmon Jr., *Adv. Corros. Sci. and Technol.*, **3**, 293 (1973).
5. C. S. Pande, M. Suenaga, B. Vyas, H. S. Isaacs, and D. F. Harling, *Scr. Metall.*, **11**, 681 (1977).
6. W. L. Clarke, R. L. Cowan, and W. L. Walker, Intergranular Corrosion of Stainless Alloys, ASTM STP 656, R. F. Steigerwald, Editor, ASTM, Philadelphia, Pennsylvania, 99 (1978).
7. W. L. Clarke and D. C. Carlson, *Mater. Peform.*, **19**, 16 (1980).
8. N. B. Gegelova, *Zashch. Met.*, **8**, 420 (1972).
9. L. A. Medvedeva, V. M. Knyazheva, Ya. M. Kolotyrkin, and S. G. Babich, *Zashch. Met.*, **11**, 699 (1975).
10. Annual Book of ASTM Standards G 108, ASTM, Philadelphia, *Pennsylvania*, 450 (1994).
11. Annual Book of JIS Standards G 0580, JIS, Tokyo, Japan, (1993).
12. A. Roelandt and J. Vereecken, *Corrosion*, **42**, 289 (1986).
13. A. Mignone, A. Borello, and A. La Barbera, *Corrosion*, **38**, 390 (1982).
14. G. L. Edgemon, M. Marek, D. F. Wilson, and G. E. C. Bell, *Corrosion*, **50**, 912 (1994).
15. Tseng-Feng Wu, Tzu-Ping Chen, and Wen-Ta Tsai, *J. Nuclear Materials*, **295**, 233 (2001).
16. Annual Book of ASTM Standards, Designation A 262 Practice A, ASTM, Philadelphia, Pennsylvania, 43 (1993).
17. G. P. Airey, A. R. Vaia, N. Pessall, and R. G. Aspden, *J. Met.*, **33**, 28 (1981).
18. E. L. Hall and C. L. Briant, Metall. Mater. Trans., A **16A**, 1225 (1985).
19. D. R. Johns and F. R. Beckitt, *Corros. Sci.*, **30**, 223 (1990).
20. A. P. Majidi and M. A. Streicher, *Corrosion*, **40**, 393 (1986).